Spectrochimica Acta Part A: Molecular and Biomolecular Spectroscopy 355 (2026) 127663

Contents lists available at ScienceDirect

Spectrochimica Acta Part A:
Molecular and Biomolecular Spectroscopy

journal homepage: www.journals.elsevier.com/spectrochimica-acta-part-a-molecular-and-biomolecular-spectroscopy

Rotational spectroscopy meets composite Pisa schemes: Structural determination of the atmospheric pollutants 1- and 2-nitronaphthalene

Shefali Baweja [a,1], Marco Mendolicchio [b], Vincenzo Barone [c,*], M. Eugenia Sanz [a,*]

[a] Department of Chemistry, King's College London, 7 Trinity Street, London SE1 1DB, United Kingdom
[b] Scuola Normale Superiore, piazza dei Cavalieri 7, 50126 Pisa, Italy
[c] INSTM, via G. Giusti 9, 50121 Firenze, Italy

HIGHLIGHTS

- The rotational spectrum of 1- and 2-nitronapthalene was recorded in the 2–8 GHz frequency range.
- Theoretical calculations have been performed using DFT and ab initio methods.
- Semi-experimental equilibrium structures were obtained for 1- and 2-nitronapthalene.

GRAPHICAL ABSTRACT

ARTICLE INFO

Keywords:
PAH
Nitronaphthalene
Rotational spectroscopy
Quantum chemical calculations
Structural determination

ABSTRACT

Polycyclic aromatic hydrocarbons (PAHs) are widespread air pollutants in the Earth's atmosphere. Understanding their structure is relevant for the study of their interactions with other atmospheric molecules and their participation in aerosol formation. Here we present the investigation of the structures of the most abundant nitrated PAHs in the atmosphere, 1-nitronaphthalene (1NN) and 2-nitronaphthalene (2NN), using high-resolution chirped pulse Fourier transform microwave spectroscopy and quantum-chemical calculations. The rotational constants, centrifugal distortion constants and ^{14}N nuclear quadrupole coupling constants for both 1NN and 2NN were determined. The observation of the heavy atom isotopologues in natural abundance led to the determination of experimental structures using substitution, effective, and mass-weighted methods. Moreover, semi-experimental equilibrium structures for 1NN and 2NN were determined by using a reduced-cost protocol based on the Pisa Composite Schemes, which combines the experimental heavy-atom isotopologue data with hydrogen atom positions and vibrational corrections obtained from affordable quantum chemical calculations. The resulting semi-experimental equilibrium structures achieve spectroscopic accuracy, demonstrating the robustness and transferability of this strategy for nitroaromatic systems. Comparison of the bond lengths and angles of 1NN and 2NN with those of related substituted naphthalenes enabled identification of common structural trends.

* Corresponding authors.
E-mail addresses: vincebarone52@gmail.com (V. Barone), maria.sanz@kcl.ac.uk (M.E. Sanz).
[1] Present address: School of Chemistry, University of Nottingham, Nottingham NG7 2RD, United Kingdom.

https://doi.org/10.1016/j.saa.2026.127663
Received 30 December 2025; Received in revised form 3 February 2026; Accepted 28 February 2026
Available online 3 March 2026

1. Introduction

Polycyclic aromatic hydrocarbons (PAHs) are classified as major environmental pollutants due to their high toxicity to humans as well as to living organisms in aquatic and terrestrial environments [1]. Direct or indirect combustion sources such as vehicles, industries, and diesel engines lead to the emission of PAHs to the atmosphere and their subsequent accumulation. Substituted PAHs are known to be more stable and toxic than their parent PAHs [2]. Among them, nitrated PAHs (NPAHs) are widespread in the atmosphere, where they are emitted from incomplete combustion of fossil fuels and biomass, as well as produced from reactions of their parent PAHs with atmospheric oxidants [3]. NPAHs have been found to be persistent in the environment, and their harmful effects include mutagenic activity, carcinogenesis, and apoptosis, among others, with much higher potency than related unsubstituted PAHs [3].

1- and 2-nitronaphthalene (1NN and 2NN, respectively) are among the most abundant NPAHS in the atmosphere [4]. They are derivatives of naphthalene where an $–NO_2$ group replaces a hydrogen atom at positions 1 and 2, respectively (see Fig. 1). During daylight, both compounds can be produced in the atmosphere via the addition of a hydroxyl radical to naphthalene, subsequently leading to a reaction with nitrogen dioxide and the removal of a water molecule [3]. During night time, they can be formed through nitrate radical addition on naphthalene followed by a reaction with nitrogen dioxide and a loss of nitric acid molecule [5,6]. A higher proportion of 1NN is formed through these reactions as compared to 2NN [5,6].

1NN and 2NN have been investigated theoretically and experimentally [4,7–14]. Experimental studies have focused on their photochemistry and photophysics. Gas-phase photolysis was found to be the main cause of degradation of 1NN and 2NN in the atmosphere [4,12–15]. Photolysis of 1NN results in a significant production of phenoxynaphthoxyl dimers, which contribute substantially to secondary organic aerosol (SOA) formation in the atmosphere and thus hold serious implications for urban air quality [16]. Photolysis rates of 1NN are an order of magnitude larger than those of 2NN [4,14]. This was attributed to different branching of the excited singlet state populated upon light irradiation between a triplet state and a singlet dissociative state [13]. The different torsional angle of the nitro group in 1NN and 2NN was proposed to play a major role in their dissimilar photodegradation behaviour [13]. It also has toxicity implications, as the longer-lived 2NN is more mutagenic. The relationship between structure and photochemical behaviour may be of relevance for other NPAHs.

In addition to their environmental relevance, 1NN and 2NN are also of interest in their role as prototypical systems for studying intramolecular charge transfer and nitro–arene interactions [17,18]. In particular, the different position of the nitro group on the naphthalene ring in 1NN and 2NN results in distinct electronic and spectroscopic properties. In comparison with 1NN, 2NN has a stronger π conjugation bonding between the nitro group and the aromatic system due to its higher dipole moment, electronic polarizability and second hyperpolarizability [7]. Moreover, the torsional angle of the $–NO_2$ group with respect to the naphthalene ring plane is predicted to be around 0° in 2NN but close to 135° in 1NN according to recent calculations [9]. However, there are no experimental reports of the structural parameters of 1NN and 2NN.

Rotational spectroscopy is a powerful tool for probing the geometry of molecules with high accuracy [19], since every molecule exhibits a distinct rotational spectrum determined by its unique mass distribution. The only requirement is for the molecule to possess a permanent dipole moment. In nitronaphthalenes, this arises from the electron-withdrawing $–NO_2$ group. Importantly, it is experimentally feasible to observe the rotational spectra of all heavy atom isotopologues (i.e., those containing ^{13}C, ^{15}N, or ^{18}O) at natural abundance, which will enable determination of the bond lengths and angles in which they participate. Deuterated isotopologues are not normally accessible under standard experimental conditions, due to the low natural abundance of deuterium (0.015%) and the lack of isotopic enrichment in typical samples.

Owing to recent hardware and software developments, quantum chemical (QC) methods have become an invaluable complement to experimental spectroscopy. Current standard practices often neglect vibrational effects and employ hybrid density functionals or second-order Møller–Plesset perturbation theory (MP2) for structure determination [20–23]. While these methods offer a reasonable balance between accuracy and computational cost, their limited intrinsic precision and the neglect of vibrational averaging effects hamper the unambiguous interpretation of high-resolution spectroscopic data in structural terms. To address their limitations, we have developed the Pisa Composite Schemes (PCS) [24], a family of QC methods designed to significantly enhance the accuracy of molecular structure predictions for medium-sized molecules at a reasonable computational cost [25]. In parallel, new models have been developed, which permit the computation of vibrational contributions at the cost of a harmonic calculation for a single isotopologue or a single anharmonic calculation to account for all isotopologues of a given molecule [26,27]. Furthermore, we have integrated the Gaussian [28] and MSR (Molecular Structure Refinement) [29] programs in a fully automated, black-box workflow, which facilitates the routine use of advanced quantum mechanical calculations in spectroscopic studies. In particular, the ground state rotational constants obtained from computed equilibrium structures and vibrational corrections of different isotopologues can be directly compared with their experimental counterparts.

Among the available techniques for gas-phase structure refinement, the semi-experimental (SE) approach is known as the most accurate, providing equilibrium geometries (r_e^{SE}) by correcting experimental rotational constants for vibrational contributions computed from quantum chemistry [30–32]. However, the high computational cost of anharmonic force fields and the need for isotopic substitution of all non-equivalent atoms often limit the practical application of this approach. The former can be addressed through the methods mentioned above, while the latter can be mitigated using constrained regressions or the

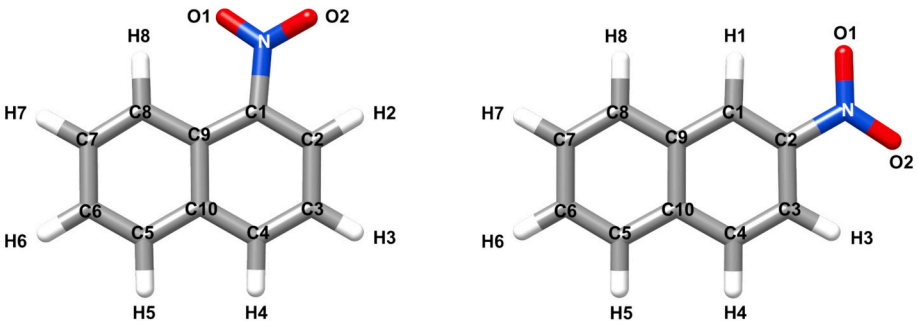

Fig. 1. Structures and atom labelling of 1-nitronaphthalene (left) and 2-nitronaphthalene (right).

Table 1
Theoretical equilibrium spectroscopic parameters for 1- and 2-nitronaphtalene using different methods with the 6–311++G(d,p) basis set.

Parameter	1NN			2NN		
	B3LYP-D3BJ	MP2	B3PW91	B3LYP-D3BJ	MP2	B3PW91
A[a] (MHz)	1364.9	1329.8	1370.3	2258.1	2238.8	2265.9
B (MHz)	745.7	751.1	747.5	496.1	492.8	497.7
C (MHz)	492.5	500.4	493.8	406.8	406.3	408.1
P_c[b] (uÅ^2)	10.84	21.47	10.71	0.00	3.70	0.00
Δ[c] (uÅ^2)	−21.67	−42.94	−21.43	0.00	−7.41	0.00
$\lvert\mu_a\rvert/\lvert\mu_b\rvert/\lvert\mu_c\rvert$[d] (D)	4.2/2.6/0.0	3.6/2.2/0.0	4.1/2.5/0.0	5.6/0.9/0.0	4.9/0.9/0.1	5.5/0.9/0.0
χ_{aa}[e] (MHz)	−0.54	−0.22	−0.51	−1.14	−0.52	−1.08
χ_{bb} (MHz)	−0.20	−0.15	−0.19	0.28	0.82	0.25
χ_{cc} (MHz)	0.73	0.37	0.70	0.86	−0.30	0.83
∠O1-N-C1-C2	147.0	130.6	147.1	–	–	–
∠O1-N-C2-C1	–	–	–	0.0	20.8	0.0

[a] A, B and C are the rotational constants.
[b] Planar moment of inertia $P_c = \sum_i m_i c_i^2$.
[c] Inertial defect $\Delta = I_c - I_a - I_b$.
[d] Absolute values of the components of the electric dipole moment along the principal inertial axes.
[e] χ_{aa}, χ_{bb} and χ_{cc} are the nuclear quadrupole coupling constants.

template molecule strategy [31–33].

In this work, we report the high-resolution rotational study of 1NN and 2NN in gas phase, combining chirped pulse Fourier transform microwave (CP-FTMW) spectroscopy [34] with QC calculations based on the BDPCS3 variant [35,36], which approaches the accuracy of coupled-cluster methods with the computational efficiency of double-hybrid functionals augmented by one-parameter bond corrections. The observation of the rotational spectra of the parent species and the heavy-atom isotopologues of 1NN and 2NN enabled determination of their experimental as well as their semi-experimental equilibrium structures. 1NN and 2NN show changes in bond lengths in comparison with naphthalene, indicating structural modifications in the naphthalene ring.

The results obtained for nitronaphthalene isomers demonstrate the effectiveness of this cost-efficient SE protocol in deriving accurate equilibrium structures from limited isotopic data. Beyond the intrinsic chemical interest of these systems, our findings provide a transferable framework for structural studies of other substituted polycyclic aromatics, highlighting the synergy between rotational spectroscopy and modern computational chemistry.

2. Methods

2.1. Experimental

The broadband rotational spectra of 1NN and 2NN were recorded in the 2–8 GHz frequency range using our chirped pulse Fourier transform microwave spectrometer at King's College London [37,38]. 1NN (99%, Apollo Scientific) and 2NN (95%, Apollo Scientific) were used without any further purification and heated to 398 K (1NN) and 410 K (2NN) to increase their concentration in the gas phase. A bespoke heating reservoir attached to the solenoid valve was used. The samples were seeded in neon as a carrier gas at a backing pressure of 5 bar and then conducted to the vacuum chamber, where the molecules expand adiabatically to form a supersonic expansion. Each molecular pulse of our target molecules, of typically 1000 μs length, was polarized by four chirped microwave pulses, each of 4 μs duration, spaced 30 μs. The resulting emission signal was collected for 20 μs after each microwave pulse as a free induction decay (FID) and stored into a fast oscilloscope. The FIDs are recorded in the time domain and then converted into the frequency domain using a fast Fourier transform algorithm. The final spectrum was obtained from averaging 3.8 MFIDs and 4.9 MFIDs for 1NN and 2NN, respectively.

2.2. Computational

1NN and 2NN are expected to be quite rigid and therefore no conformational sampling was necessary. Initially the B3LYP hybrid density functional [39,40], augmented by the D3BJ empirical dispersion [41,42], and the MP2 [43] wave-function model with Pople's 6–311++G(d,p) basis set were employed to optimise their geometries. However, predicted ^{14}N nuclear quadrupole coupling constants (NQCC) showed large differences. It has been reported that the NQCCs of the –NO_2 group are not well described by MP2 [44–47]. Hence, additional calculations were performed using the B3PW91 functional [48], which is known to yield accurate values of NQCCs for molecules with ^{14}N, including those with nitro groups [44,47,48]. The spectroscopic parameters of the theoretical structures, including the rotational and NQCCs constants, and the dipole moment components, predicted by the methods above are collected in Table 1.

Spectroscopic parameters from calculations refer to equilibrium structures (A^{eq}, B^{eq}, C^{eq}) while the experimental ones correspond to effective structures in the ground vibrational state (A^0, B^0, C^0) [19]. Therefore, proper comparison between experimental and quantum-chemistry data requires accounting for the couplings between rotations and vibrations (broadly referred to as vibrational corrections) needed to go from equilibrium to ground state parameters. In the framework of vibrational perturbation theory to second order (VPT2), the computation of vibrational corrections requires harmonic frequencies (ω_i), Coriolis couplings ($\zeta_{ij,\tau}$) and, above all, semi-diagonal third derivatives of the energy with respect to normal modes (f_{ij}) [26,33].

A two-tier approach was followed to calculate vibrational corrections while ensuring cost-efficiency. First, molecular structures are optimized using B3LYP-D3BJ [39–42] in conjunction with the 6–31+G* basis set [49–51] (hereafter HPCS2). Then, the geometrical parameters are refined with the revDSD-PBEP86 double hybrid functional [52] augmented by the D3BJ empirical dispersion [41,42] in conjunction with the 3F12− basis set [53], which is obtained from its standard cc-pVTZ-F12 (3F12) counterpart [54] by removing d functions on first-row atoms and replacing the two f functions on second- and third-row atoms by a single f function taken from the cc-pVTZ basis set [55]. This combination of density functional, basis set, and dispersion corrections will be referred to as DPCS3 in the following. In addition to geometrical parameters [56], it is well documented that the DPCS3 model provides remarkably accurate centrifugal-distortion constants [57], dipole moments [58], and nuclear quadrupole coupling constants [59].

The magnitude of vibrational corrections is typically between 0.3 and 0.7% of the corresponding equilibrium rotational constants. Since the relative errors of vibrational corrections computed at the HPCS2 level are usually of the order of 10%, the ensuing error on the rotational

constants is more than acceptable. At the same time, equilibrium geometries computed at the DPCS3 level are remarkably accurate but need further refinement to reach spectroscopic accuracy. In particular, the application of bond corrections to DPCS3 geometries (respectively referred to as Δr_{ij}^{BCV} for the core-valence (CV) contribution and Δr_{ij}^{BV} for the valence contribution) leads to the very accurate BDPCS3 model:

$$r_{ij}(\mathrm{BDPCS3}) = r_{ij}(\mathrm{DPCS3}) + \Delta r_{ij}^{CV} + \Delta r_{ij}^{BCV}$$

with

$$\Delta r_{ij}^{BCV} = K_{ni,nj}$$

and

$$\Delta r_{ij}^{BV} = K'_{ni,nj}\, r_{ij}(\mathrm{DPCS3})$$

where n_i and n_j are the atomic numbers of atoms involved in the bond. One-parameter corrections for all bond lengths can be obtained relating $K_{ni,nj}$ to the covalent radii of the atoms and $K'_{ni,nj}$to the Pauling bond order [25,35,36]. A statistical comparison of 286 C–H bonds from the SE111 database [25] showed that DPCS3 geometries exhibit a consistent overestimation of C–H bond lengths, with an average deviation which is more than twice the magnitude of the current BDPCS3 correction. To account for this, we applied a uniform reduction of 0.0025 Å to the DPCS3 C–H bond lengths. Note that the BDPCS3 results can be obtained at the same cost as the underlying DPCS3 geometry optimization.

All the quantum-chemistry computations have been performed with the Gaussian16 package [28] and the BDPCS3 geometrical parameters have been obtained by a public domain web site (https://www.skies-village.it/proxima/pcsbonds/).

3. Results

3.1. Spectral analysis

The rotational spectra of 1NN and 2NN showed intense lines in the 2–8 GHz frequency region (see Fig. S1). The theoretical rotational constants and dipole moment values listed in Table 1 informed our initial searches for rotational transition patterns corresponding to each molecule. Both 1NN and 2NN had large values predicted for the μ_a dipole moment component (~4.2 D and ~5.6 D, respectively), and thus we first searched for R-branch *a*-type transitions. A set of intense *a*-type $J+1 \leftarrow J$ transitions showing the expected spectral patterns was identified for each of 1NN and 2NN through the AUTOFIT [60,61] feature incorporated in the program PGOPHER [61,62]. Our assignments of both 1NN and 2NN were confirmed through the measurement of additional *a*- and *b*-type transitions. The relative intensities of the transitions, with strong *a*-type and weaker *b*-type lines, were consistent with the

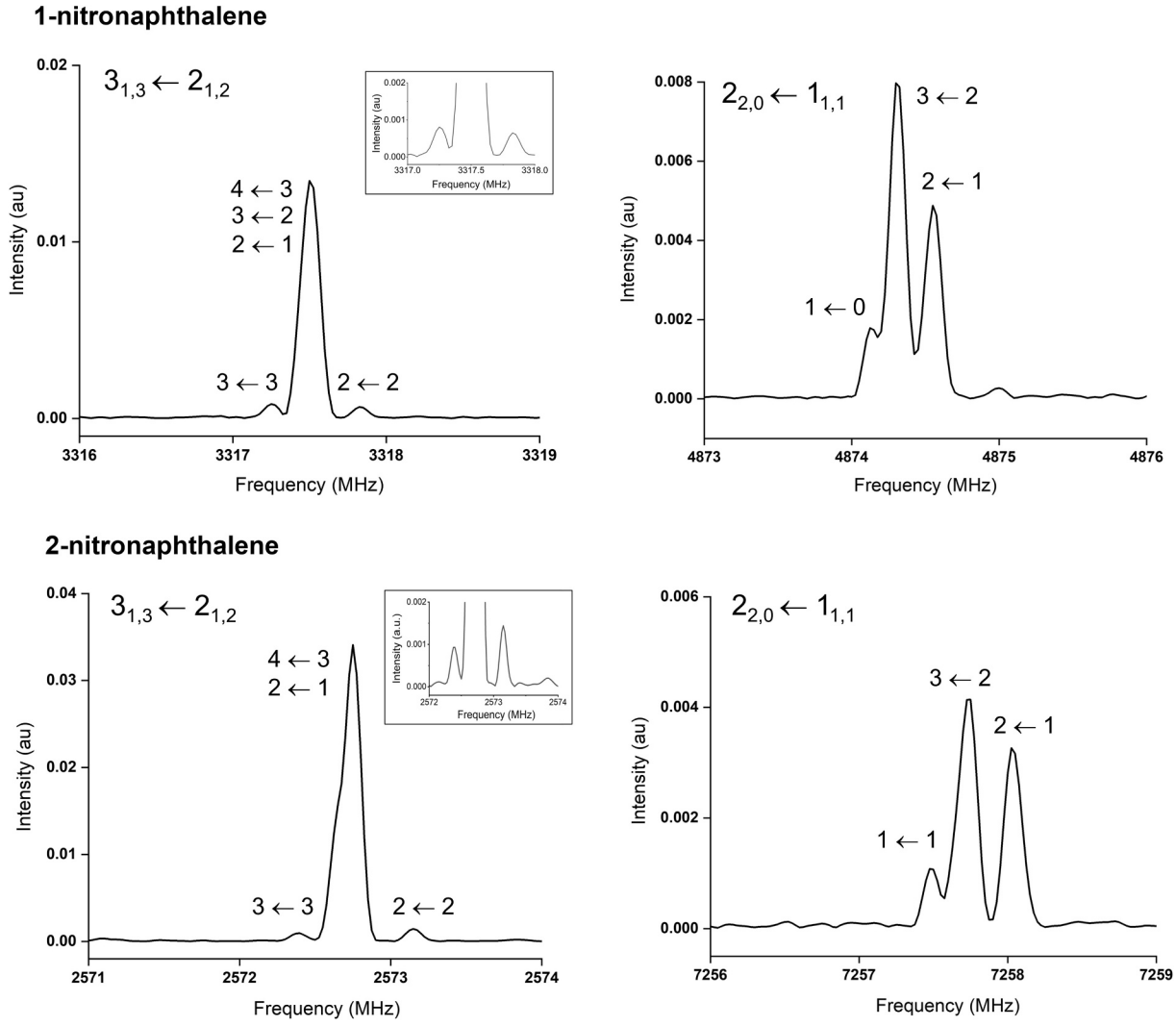

Fig. 2. Sections of the broadband rotational spectrum showing the ^{14}N nuclear hyperfine splittings observed for the *a*-type $3_{1,3} \leftarrow 2_{1,2}$ (enlarged region shows the weaker $F' \leftarrow F''$ components) and the *b*-type $2_{2,0} \leftarrow 1_{1,1}$ rotational transitions of 1-nitronaphthalene (top) and 2-nitronaphthalene (bottom).

predicted dipole moment values.

Each transition of both nitronaphthalenes was split into several components due to the presence of a quadrupole ^{14}N nucleus. However, some of the rotational transitions, especially *a*-type ones, showed the three most intense $F + 1 \leftarrow F$ components blended as an intense peak, with the two less intense $F \leftarrow F$ components featured on either side (Fig. 2). Using Pickett's SPFIT/SPCAT programs [63], the measured hyperfine components were fit to Watson A-reduced semirigid rotor Hamiltonian in the I^r representation [64] supplemented by an additional term to give account of the nuclear quadrupole coupling splitting [19]. The experimental spectroscopic parameters of 1NN and 2NN determined from the fits are compiled in Tables 2 and 3. For 2NN, no centrifugal distortion constants were determined when floated.

The high intensity of the transitions allowed to observe ^{13}C and ^{15}N isotopologues in natural abundances (1.1% and 0.4%, respectively), and also the ^{18}O isotopologues (0.2% natural abundance) for 2NN. The transitions arising from the isotopologues were observed at the expected frequency shifts from the parent species, and were fitted to the same Hamiltonian. For the ^{13}C species, only the most intense nuclear quadrupole coupling hyperfine component was observed for each transition, and therefore the NQCCs were fixed in the fits to those determined for the corresponding parent species. The obtained rotational constants are collected in Tables 2 and 3.

3.2. Structural determination

The different position of the $–NO_2$ substituent in 1NN and 2NN results in a significant change in their structures. Their inertial defects, determined from the principal moments of inertia using the relation $\Delta = I_c - I_a - I_b$, are dramatically different (Tables 2 and 3). For 1NN, $\Delta = -28.916(3)$ uÅ^2, while for 2NN, $\Delta = -0.765(1)$ uÅ^2. Values of the inertial defect close to zero are taken as an indication of planarity [19]. The small negative value for 2NN is consistent with it being planar and with similar values of Δ for other PAHs, caused by their low-frequency out-of-plane vibrations [65–67]. Moreover, the values of the experimental planar moments of inertia P_c for 2NN and its isotopologues are nearly invariant (see Table 3). Since P_c informs on the mass distribution out of the *ab* inertial plane, this indicates that all the substituted atoms (carbons, nitrogen and oxygens) are on the *ab* plane. All density functional methods predict a equilibrium planar structure of 2NN in agreement with experimental observations, with virtually zero values for the inertial defect from the equilibrium rotational constants (see Tables 1 and 4). MP2, however, predicts $\Delta = -7.41$ uÅ^2. This indicates a significant out-of-plane contribution, arising from a rotation of the $–NO_2$ group, which adopts a ∠O1-N-C2-C1 dihedral angle of 20.8°. The BDPCS3 method including vibrational corrections computed at the HPCS2 level (P^0 (Best) in Table 4), described below, returns $\Delta = -1.02$ uÅ^2, remarkably close to the experimental value.

The experimental inertial defect of 1NN shows that it is non-planar. The P_c values of the parent species, ^{13}C and ^{15}N isotopologues display minimal changes (see Tables 2 and 3), thus implying that the carbon and nitrogen nuclei are located on the ring plane, and that non-planarity arises from the $–NO_2$ group. A relaxed potential energy scan of the ∠O1-N-C1-C2 dihedral angle of 1NN using B3LYP-D3BJ/6–311++G(d, p) confirms that the planar configuration is *ca.* 3 kJ mol^{-1} above the global minimum (see Fig. S2). In fact, all theoretical methods predict the $–NO_2$ group to be out of plane, with values of the ∠O1-N-C1-C2 dihedral angle of 147.0° (B3LYP-D3BJ), 130.6° (MP2), 147.1° (B3PW91). B3LYP-D3BJ, MP2 and B3PW91 predict the 1NN inertial defect values as −21.67 uÅ^2, −42.94 uÅ^2 and −21.43 uÅ^2, respectively, while the experimental value lies between these predictions, but it is closer to the density functional theory values. Including vibrational corrections within the BDPCS3 method achieves excellent results, with an inertial defect of −28.96 uÅ^2 (Table 5), which corresponds to a torsional angle

Table 2
Experimental spectroscopic parameters of the parent, ^{13}C and ^{15}N isotopologues of 1-nitronaphthalene.

Parameter	Parent	$^{13}C_1$	$^{13}C_2$	$^{13}C_3$	$^{13}C_4$	$^{13}C_5$
A[a] (MHz)	1353.89427(73)[g]	1353.625(14)	1344.6001(67)	1330.2952(90)	1337.295(18)	1353.460(17)
B (MHz)	748.56249(32)	747.50019(84)	746.6170(12)	748.4548(13)	747.3509(31)	740.4218(12)
C (MHz)	495.71519(33)	495.22913(51)	493.61058(30)	492.47452(47)	492.93768(40)	492.06718(50)
Δ_J (kHz)	0.0120(40)	[0.0120][h]	[0.0120]	[0.0120]	[0.0120]	[0.0120]
δ_K (kHz)	0.127(45)	[0.127]	[0.127]	[0.127]	[0.127]	[0.127]
P_c[b] (uÅ^2)	14.4580(34)	14.4746(20)	14.4543(11)	14.4632(15)	14.4497(29)	14.4503(25)
$a/b/c$[c] (D)	y/y/n	y/n/n	y/n/n	y/n/n	y/n/n	y/n/n
χ_{aa}[d] (MHz)	−0.4881(64)	[−0.4881]	[−0.4881]	[−0.4881]	[−0.4881]	[−0.4881]
χ_{bb} (MHz)	−0.1631(81)	[−0.1631]	[−0.1631]	[−0.1631]	[−0.1631]	[−0.1631]
χ_{cc} (MHz)	0.6512(81)	[0.6512]	[0.6512]	[0.6512]	[0.6512]	[0.6512]
N[e]	115	11	7	8	7	10
σ[f] (kHz)	8.0	8.1	4.5	6.7	5.2	7.4
Parameter	**$^{13}C_6$**	**$^{13}C_7$**	**$^{13}C_8$**	**$^{13}C_9$**	**$^{13}C_{10}$**	**^{15}N**
A[a] (MHz)	1350.7658(69)[g]	1340.748(20)	1345.0201(74)	1353.804(19)	1351.670(14)	1352.389(17)
B (MHz)	738.29994(60)	743.9070(12)	747.99734(68)	748.4631(13)	746.5180(10)	743.56915(98)
C (MHz)	490.78745(33)	491.92709(78)	494.28183(36)	495.66460(57)	494.52395(57)	493.33088(75)
Δ_J (kHz)	[0.0120]	[0.0120][h]	[0.0120]	[0.0120]	[0.0120]	[0.0120]
δ_K (kHz)	[0.127]	[0.127]	[0.127]	[0.127]	[0.127]	[0.127]
P_c[b] (uÅ^2)	14.4644(11)	14.4753(48)	14.4663(11)	14.4633(27)	14.4617(21)	14.4690(26)
$a/b/c$[c] (D)	y/n/n	y/n/n	y/n/n	y/n/n	y/n/n	y/n/n
χ_{aa}[d](MHz)	[−0.4881]	[−0.4881]	[−0.4881]	[−0.4881]	[−0.4881]	–
χ_{bb} (MHz)	[−0.1631]	[−0.1631]	[−0.1631]	[−0.1631]	[−0.1631]	–
χ_{cc} (MHz)	[0.6512]	[0.6512]	[0.6512]	[0.6512]	[0.6512]	–
N[e]	12	10	11	11	13	8
σ[f] (kHz)	6.1	11.4	6.8	8.9	9.4	9.3

[a] A, B and C are the rotational constants, Δ_J and δ_K are the quartic centrifugal distortion constants.
[b] Planar moment of inertia $P_c = \sum_i m_i c_i^2$.
[c] Yes (y) or no (n) observation of μ_a-, μ_b- and μ_c- type transitions.
[d] χ_{aa}, χ_{bb} and χ_{cc} are the ^{14}N nuclear quadrupole coupling constants.
[e] N is the number of the fitted hyperfine components.
[f] σ is the rms deviation of the fit.
[g] Standard error in parentheses in units of the last digit.
[h] Values in square brackets are fixed to those of the parent species.

Table 3
Experimental spectroscopic parameters of the parent, ^{13}C, ^{15}N and ^{18}O isotopologues of 2-nitronaphthalene.

Par.	Parent	$^{13}C_1$	$^{13}C_2$	$^{13}C_3$	$^{13}C_4$	$^{13}C_5$	$^{13}C_6$
A[a] (MHz)	2252.8043(11)[g]	2244.648(42)	2252.751(40)	2231.461(50)	2220.349(50)	2239.646(46)	2252.575(49)
B (MHz)	496.08294(16)	496.00566(35)	495.18474(34)	495.56595(45)	496.04548(45)	492.59400(40	489.69563(39)
C (MHz)	406.80652(12)	406.48822(33)	406.20058(32)	405.75897(41)	405.71297(41)	404.03234(37)	402.49339(37)
P_c[b] (uÅ^2)	−0.76476(40)	−0.7670(32)	−0.7642(21)	−0.7654(26)	−0.7718(27)	−0.7677(24)	−0.7623(25)
$a/b/c$ [c](D)	y/y/n	y/n/n	y/n/n	y/n/n	y/n/n	y/n/n	y/n/n
χ_{aa}[d] (MHz)	−1.0621(33)	[−1.0621][h]	[−1.0621]	[−1.0621]	[−1.0621]	[−1.0621]	[−1.0621]
χ_{bb} (MHz)	0.2244(58)	[0.2244]	[0.2244]	[0.2244]	[0.2244]	[0.2244]	[0.2244]
χ_{cc} (MHz)	0.8377(58)	[0.8377]	[0.8377]	[0.8377]	[0.8377]	[0.8377]	[0.8377]
N[e]	190	22	23	22	22	20	24
σ[f] (kHz)	8.5	6.9	6.6	8.3	8.2	7.6	7.7
Par.	**$^{13}C_7$**	**$^{13}C_8$**	**$^{13}C_9$**	**$^{13}C_{10}$**	**^{15}N**	**$^{18}O_1$**	**$^{18}O_2$**
A[a] (MHz)	2238.610(44)[g]	2228.934(47)	2249.720(49)	2246.198(37)	2252.134(26)	2212.178(57)	2244.851(63)
B (MHz)	490.91400(35)	494.24530(40)	495.67092(41)	495.25689(32)	492.32970(20)	487.00271(48)	483.73491(51)
C (MHz)	402.87043(33)	404.78986(38)	406.42888(37)	406.03668(30)	404.25742(19)	399.37464(48)	398.22051(37)
P_c[b] (uÅ^2)	−0.7757(23)	−0.7650(25)	−0.7643(25)	−0.7678(19)	−0.7637(13)	−0.7607(31)	−0.7784(33)
$a/b/c$ [c](D)	y/n/n	y/n/n	y/n/n	y/n/n	y/n/n	y/n/n	y/n/n
χ_{aa}[d] (MHz)	[−1.0621][h]	[−1.0621]	[−1.0621]	[−1.0621]	–	[−1.0621]	[−1.0621]
χ_{bb} (MHz)	[0.2244]	[0.2244]	[0.2244]	[0.2244]	–	[0.2244]	[0.2244]
χ_{cc} (MHz)	[0.8377]	[0.8377]	[0.8377]	[0.8377]	–	[0.8377]	[0.8377]
N[e]	23	23	22	21	22	13	13
σ[f] (kHz)	6.9	7.8	7.6	6.0	3.9	7.6	6.7

[a] A, B and C are the rotational constants.
[b] Planar moment of inertia $P_c = \sum_i m_i c_i^2$.
[c] Yes (y) or no (n) observation of μ_a-, μ_b- and μ_c- type transitions.
[d] χ_{aa}, χ_{bb} and χ_{cc} are the ^{14}N nuclear quadrupole coupling constants.
[e] N is the number of the fitted hyperfine components.
[f] σ is the rms deviation of the fit.
[g] Standard error in parentheses in units of the last digit.
[h] Values in square brackets are fixed to those of the parent species.

Table 4
Comparison between the experimental and computed ground-state rotational constants (in MHz), nuclear quadrupole coupling constants (in MHz), and dipole moment components (in Debye) of 2-nitronaphthalene.

	P^{eq} (HPCS2)	P^{eq} (BDPCS3)	ΔP^{vib} (HPCS2)	P^0 (HPCS2)	P^0 (Best)	Exp.
A	2250.4	2269.8	−16.0	2234.4	2253.8	2252.8043
B	495.7	499.2	−3.2	492.5	495.9	496.08294
C	406.2	409.2	−2.5	403.8	406.7	406.80652
max%[a]	–	–	–	0.81	0.04	–
mue%[b]	–	–	–	0.76	0.03	–
χ_{aa}	−1.08	−1.03	−0.02	−1.10	−1.05	−1.0621
χ_{bb}	0.31	0.30	−0.00	0.30	0.23	0.2244
χ_{cc}	0.78	0.73	0.03	0.80	0.76	0.8376
μ_a	−5.2	−5.0	0.1	−5.2	−4.9	y
μ_b	0.8	0.9	0.0	0.8	0.8	y
μ_c	0.0	0.0	0.0	0.0	0.0	n

[a] Maximum absolute percentage error of the theoretical rotational constants with respect to their experimental counterparts. [b] Mean unsigned relative error of the theoretical rotational constants with respect to their experimental counterparts.

Table 5
Comparison between the experimental and computed ground-state rotational constants (in MHz), nuclear quadrupole coupling constants (in MHz), and dipole moment components (in Debye) of 1-nitronaphthalene.

	P^{eq} (HPCS2)	P^{eq} (BDPCS3)	ΔP^{vib} (HPCS2)	P^0 (HPCS2)	P^0 (Best)	Exp.
A	1370.0	1364.2	−9.5	1360.4	1354.7	1353.89427
B	742.3	752.9	−4.8	737.5	748.0	748.56249
C	488.2	498.7	−3.1	485.0	495.6	495.71519
max%[a]	–	–	–	2.1	0.1	–
mue%[b]	–	–	–	1.4	0.0	–
χ_{aa}	−0.53	−0.46	0.01	−0.52	−0.45	−0.49
χ_{bb}	−0.17	−0.16	−0.02	−0.19	−0.19	−0.17
χ_{cc}	0.70	0.62	0.01	0.71	0.63	0.65
μ_a	−4.0	−3.7	0.1	−3.9	−3.66	y
μ_b	2.4	2.3	0.0	2.4	2.25	y
μ_c	0.0	0.0	0.0	0.0	0.01	n

[a] Maximum absolute percentage error of the theoretical rotational constants with respect to their experimental counterparts. [b] Mean unsigned relative error of the theoretical rotational constants with respect to their experimental counterparts.

for the $–NO_2$ group of 141.5°.

We used different structural determination methods to obtain the structural parameters of 1NN and 2NN, taking advantage of the observation of isotopically substituted species. The coordinates of the substituted atoms in the principal inertial axis system were obtained by applying Kraitchman's equations [68] as implemented in the program KRA [69] (Tables S2-S3). Structural parameters were then computed using the program EVAL [69], leading to partial r_s substitution structures (Tables 6 and 7). A caveat of r_s structures is that substitution coordinates with small values (corresponding to atoms located close to the principal inertial axes) are typically affected by large errors, and so are the structural parameters derived from them. For 1NN, all atoms have small values for the *c* coordinate, as only the oxygen atoms of the $–NO_2$ group are off the molecular plane. The *c* coordinates of C2, C4 and C5 were fixed to zero as applying Kraitchman's equations returned imaginary values (Table S2). In addition, C9 has small values for all three *a*, *b* and *c* coordinates, and C1 and C5 have small values for the *b* coordinate (Table S2). For 2NN, a planar molecule, any two pairs of moments of inertia can be used to determine structural parameters, but their results will be slightly different as the inertial defect is not zero. Therefore, and considering that the inertial defect of 2NN is relatively large, with a value of $\Delta = -0.765(1)$ uÅ^2, we calculated the r_s coordinates from each of the two pairs and average their values (Table S3). In 2NN, C1 and C4 have small *a* coordinates while C2 and C6 have small *b* coordinates.

We also determined the effective r_0 structure for 1NN and the mass-dependent $r_m^{(1)}$ structure for 2NN [70] through least-squares fits of the experimental ground state moments of inertia of their parent and observed isotopologues using the program STRFIT [69] (Tables S4 and S5). It was not possible to obtain a comparably good fit for the r_0 structure 2NN without the inclusion of the mass-dependent term that considers the contributions of the vibrations from the various isotopomers to the moments of inertia.

Additionally, we calculated the semi-experimental equilibrium (SE) structures to account for the vibrational effects which cause the difference between equilibrium (A^{eq}, B^{eq}, C^{eq}) and experimental ground-state (A^0, B^0, C^0) rotational constants. We followed an approach that was found to be optimal for nitrobenzene, which was used as a benchmark system (see details in the SI). Nitrobenzene is a simple nitroaromatic compound for which the rotational spectra of all its isotopologues, including the hydrogen atoms, had been observed [71]. This allowed us

Table 6
Experimental, theoretical and semi-experimental equilibrium structural parameters of 2-nitronaphthalene (distances in Å, angles in degrees).

Parameter	r_s	$r_m^{(1)}$	HPCS2	DPCS3	BDPCS3	SE[c,d,e]
r(C1-C2)	1.372(22)	1.366(6)[a]	1.3746	1.3696	1.3675	1.366(3)
r(C2-C3)	1.433(30)	1.406(7)	1.4129	1.4104	1.4082	1.4095
r(C3-C4)	1.348(8)	1.380(8)	1.3727	1.3707	1.3690	1.369(2)
r(C4-C10)	1.436(6)	1.427(8)	1.4217	1.4195	1.4173	1.418(2)
r(C5-C10)	1.4242(18)	1.421(3)[a]	1.4179	1.4172	1.4152	1.414(1)
r(C5-C6)	1.388(12)	1.373(6)	1.3768	1.3732	1.3714	1.372(2)
r(C6-C7)	1.406(16)	1.422(7)	1.4163	1.4148	1.4126	1.414(2)
r(C7-C8)	1.3766(13)	1.375(3)	1.3750	1.3723	1.3706	1.3706(9)
r(C8-C9)	1.431(4)	1.428(4)	1.4202	1.4187	1.4164	1.418(1)
r(C9-C1)	1.366(5)	1.408(7)	1.4150	1.4152	1.4129	1.413(3)
r(C9-C10)	1.421(5)	1.421(7)	1.4338	1.4242	1.4219	1.423(2)
r(N-C2)	1.476(7)	1.481(3)	1.4683	1.4710	1.4682	1.467(2)
r(O1-N)	1.233(7)	1.221(3)	1.2310	1.2241	1.2215	1.220(1)
r(O2-N)	1.221(6)	1.2271(3)	1.2314	1.2248	1.2222	1.222(2)
r(H1-C1)	–	1.0816[b]	1.0834	1.0819	1.0794	1.0794[f]
r(H3-C3)	–	1.0803[b]	1.0820	1.0802	1.0877	1.0877[f]
r(H4-C4)	–	1.0839[b]	1.0860	1.0841	1.0816	1.0816[f]
r(H5-C5)	–	1.0842[b]	1.0866	1.0844	1.0819	1.0819[f]
r(H6-C6)	–	1.0837[b]	1.0860	1.0834	1.0809	1.0809[f]
r(H7-C7)	–	1.0833[b]	1.0858	1.0833	1.0808	1.0808[f]
r(H8-C8)	–	1.0841[b]	1.0865	1.0843	1.0818	1.0818[f]
∠ (O1-N-C2)	116.6(12)	118.10(14)	117.94	117.88	117.88	117.95(3)
∠ (O2-N-C2)	119.2(13)	117.5(3)[a]	117.49	117.37	117.37	117.44(3)
∠ (N-C2-C3)	116.4(14)	117.8(2)	118.66	118.53	118.53	118.54(5)
∠ (C1-C2-C3)	122.1(6)	123.5(3)[a]	122.52	122.72	122.72	122.7(1)
∠ (C2-C3-C4)	118.2(3)	118.0(2)	118.67	118.55	118.55	118.54(2)
∠ (C3-C4-C10)	121.1(2)	121.0(2)	121.24	121.15	121.15	121.14(2)
∠ (C4-C10-C9)	118.5(3)	118.9(3)	119.01	119.13	119.13	119.12(2)
∠ (C10-C9-C1)	120.4(3)	119.7(4)	119.07	119.22	119.22	119.22(2)
∠ (C5-C6-C7)	120.6(3)	120.36(16)	120.54	120.46	120.46	120.46(2)
∠ (C6-C7-C8)	120.4(2)	120.19(18)	120.26	120.31	120.31	120.31(2)
∠ (C7-C8-C9)	120.8(2)	120.6(3)	120.55	120.42	120.42	120.41(2)
∠ (C8-C9-C10)	118.7(2)	118.8(4)	119.20	119.30	119.30	119.28(2)
∠ (C9-C1-C2)	119.8(9)	118.9(4)[a]	119.46	119.21	119.21	119.3(1)
∠(H1-C1-C9)	–	120.76[b]	120.81	120.75	120.75	120.75[f]
∠ (H3-C3-C4)	–	122.05[b]	122.18	121.99	121.99	121.99[f]
∠ (H4-C4-C10)	–	118.85[b]	118.76	118.90	118.90	118.90[f]
∠ (H5-C5-C6)	–	120.44[b]	120.53	120.51	120.51	120.51[f]
∠ (H6-C6-C7)	–	119.48[b]	119.49	119.54	119.54	119.54[f]
∠ (H7-C7-C6)	–	119.60[b]	119.60	119.61	119.61	119.61[f]
∠ (H8-C8-C7)	–	120.64[b]	120.71	120.68	120.68	120.68[f]
σ[g]		0.034	–	–	–	0.01

[a] Derived parameter.
[b] Fixed to the B3LYP-D3BJ/6–311++G(d,p) value.
[c] Vibrational corrections at the HPCS2 level of theory.
[d] Fit performed employing the *A* and *B* rotational constants of each isotopic species, equally weighted.
[e] SE structure obtained starting from the BDPCS3 geometry and optimizing the C–C–C and dihedral angles classes, and the other parameters separately.
[f] Fixed to the DPCS3 value.
[g] Standard deviation of the fit (in MHz).

Table 7
Experimental, theoretical and semi-experimental equilibrium structural parameters of 1-nitronaphthalene (distances in Å, angles in degrees).

Parameter	r_s	r_0	HPCS2	DPCS3	BDPCS3	SE[c,d]
r(C1-C2)	1.423(8)	1.395(15)	1.3788	1.3715	1.3698	1.383(6)
r(C2-C3)	1.406(5)	1.397(12)	1.4068	1.4081	1.4060	1.407(3)
r(C3-C4)	1.408(6)	1.412(6)	1.3753	1.3718	1.3701	1.373(3)
r(C4-C10)	1.413(3)	1.409(7)	1.4180	1.4175	1.4152	1.407(3)
r(C10-C5)	1.435(3)	1.427(5)	1.4195	1.4184	1.4162	1.419(2)
r(C5-C6)	1.348(6)	1.371(5)[a]	1.3736	1.3706	1.3689	1.374(3)
r(C6-C7)	1.417(2)	1.414(5)	1.4128	1.4125	1.4103	1.408(3)
r(C7-C8)	1.382(3)	1.376(7)[a]	1.3773	1.3733	1.3713	1.372(3)
r(C8-C9)	1.498(15)	1.444(13)	1.4212	1.4202	1.4180	1.428(4)
r(C9-C1)	1.320(9)	1.376(15)[a]	1.4306	1.4234	1.4214	1.415(4)
r(C9-C10)	1.413(11)	1.431(19)	1.4385	1.4284	1.4261	1.424(4)
r(N-C1)	1.461(5)	1.483(12)	1.4714	1.4700	1.4672	1.456(4)
r(O1-N)	–	1.226(8)[a]	1.2325	1.2256	1.2230	1.2230[e]
r(O2-N)	–	1.225(13)[a]	1.2316	1.2247	1.2221	1.2221[e]
r(H2-C2)	–	1.0811[b]	1.0824	1.0815	1.0790	1.0790[e]
r(H3-C3)	–	1.0827[b]	1.0850	1.0826	1.0801	1.0801[e]
r(H4-C4)	–	1.0843[b]	1.0800	1.0844	1.0819	1.0819[e]
r(H5-C5)	–	1.0842[b]	1.0866	1.0843	1.0818	1.0818[e]
r(H6-C6)	–	1.0834[b]	1.0858	1.0832	1.0807	1.0807[e]
r(H7-C7)	–	1.0836[b]	1.0860	1.0833	1.0808	1.0808[e]
r(H8-C8)	–	1.0783[b]	1.0794	1.0793	1.0768	1.0768[e]
∠ (C1-C2-C3)	118.4(4)	119.0(5)	120.27	119.70	119.70	119.72(1)
∠ (C2-C3-C4)	119.4(2)	119.7(3)	119.64	119.79	119.79	119.80(1)
∠ (C3-C4-C10)	119.8(2)	120.1(4)	121.24	121.10	121.10	121.11(1)
∠ (C4-C10-C9)	118.0(5)	120.1(7)[a]	120.23	120.18	120.18	120.19(1)
∠ (C10-C5-C6)	121.6(3)	120.58(3)	120.95	120.79	120.80	120.79(1)
∠ (C5-C6-C7)	119.65(10)	119.7(2)[a]	119.61	119.83	119.83	119.84(1)
∠ (C8-C9-C10)	114.5(6)	117.1(8)	118.11	118.62	118.62	118.63(1)
∠ (C9-C10-C5)	121.9(6)	120.2(4)	119.44	119.31	119.31	119.32(1)
∠ (C9-C1-C2)	120.7(7)	123.6(10)[a]	122.48	123.00	122.98	122.2(4)
∠ (N-C1-C2)	112.7(3)	114.4(4)	115.37	115.94	115.94	115.9(1)
∠ (O1-N-C1)	–	119.0(12)	118.64	117.94	117.94	117.94[e]
∠ (O2-N-O1)	–	124.3(14)[a]	123.87	124.76	124.76	124.76[e]
∠ (H2-C2-C1)	–	119.00[b]	118.70	119.16	119.16	119.16[e]
∠ (H3-C3-C2)	–	119.52[b]	119.56	119.52	119.52	119.52[e]
∠ (H4-C4-C3)	–	120.34[b]	120.40	120.42	120.42	120.42[e]
∠ (H5-C5-C10)	–	118.43[b]	118.33	118.50	118.50	118.50[e]
∠ (H6-C6-C5)	–	120.36[b]	120.39	120.28	120.28	120.28[e]
∠ (H7-C7-C6)	–	119.55[b]	119.55	119.59	119.59	119.59[e]
∠ (H8-C8-C9)	–	119.57[b]	119.29	119.78	119.78	119.78[e]
τ(C1-C2-C3-C4)	−12.6(34)	−1.2(3)[a]	−1.01	−1.29	−1.29	−1.281(1)
τ (C2-C3-C4-C10)	9.7(36)	−0.27(27)[a]	−0.26	−0.25	−0.25	−0.236(1)
τ(C3-C4-C10-C9)	−5.7(39)	1.3(2)[a]	1.06	1.33	1.33	1.351(1)
τ (C4-C10-C9-C8)	−170.3(23)	−178.7(12)[a]	−178.69	−178.49	−178.49	−178.476(1)
τ (C10-C5-C6-C7)	−1.2(33)	0.22(10)[a]	−0.15	−0.14	−0.13	−0.124(1)
τ (C8-C9-C10-C5)	4.5(39)	0.86(17)[a]	0.96	1.14	1.14	1.159(1)
τ (C9-C10-C5-C6)	−1.5(4)	−0.82(14)[a]	−0.66	−0.77	−0.77	−0.764(1)
τ (N-C1-C2-C3)	−177.0(20)	−178.2(2)[a]	−178.08	−177.88	−177.88	−177.866(1)
τ (O1-N-C1-C2)	–	141.18(4)	153.50	141.45	141.45	141.45[e]
τ (O2-N-O1-C1)	–	178.6(11)[a]	178.46	178.39	178.39	178.39[e]
τ (H5-C5-C10-C9)	–	179.77[b]	179.73	179.63	179.63	179.63[e]
τ (H6-C6-C5-C10)	–	−179.74[b]	−179.84	−179.84	−179.84	−179.84[e]
τ (H7-C7-C6-C5)	–	−179.79[b]	−179.46	−179.43	−179.43	−179.43[e]
τ (H8-C8-C9-C1)	–	2.78[b]	1.87	2.48	2.48	2.48[e]
τ (H2-C2-C1-C9)	–	−178.67[b]	−179.01	−178.79	−178.79	−178.79[e]
τ (H3-C3-C2-C1)	–	178.69[b]	178.88	178.69	178.69	178.69[e]
τ (H4-C4-C3-C2)	–	−179.83[b]	−179.96	−179.81	−179.81	−179.81[e]
σ[f]		0.027	–	–	–	0.03

[a] Derived parameter.
[b] Fixed to the B3LYP-D3BJ/6–311++G(d,p) value.
[c] Vibrational corrections at the HPCS2 level of theory.
[d] SE structure obtained starting from the BDPCS3 geometry and optimizing the C–C–C and dihedral angles classes, and the other parameters separately.
[e] Fixed to the DPCS3 value.
[f] Standard deviation of the fit (in MHz).

to obtain a complete SE equilibrium structure by applying vibrational corrections computed at the HPCS2 level to the BDPCS3 structural parameters. However, a reduced-dimensionality SE fit in which the hydrogen atoms are fixed at their BDPCS3 positions yielded a more stable final structure (Table S1). The same method was applied to 1NN and 2NN.

The equilibrium geometries of 1NN and 2NN have been computed at both the HPCS2 and BDPCS3 levels of theory, along with the values of the properties of interest, namely, rotational constants, NQCCs, and dipole moment components. Vibrational corrections to these properties computed at the HPCS2 level and combined with their equilibrium BDPCS3 counterparts provide the best estimate of the ground-state properties:

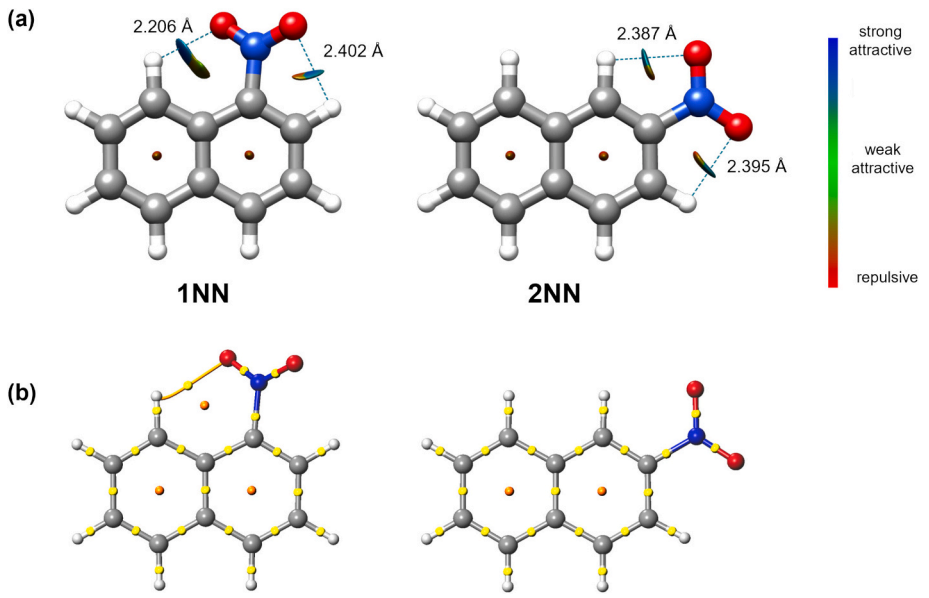

Fig. 3. **(a)** Structures of 1-nitronaphthalene (1NN) and 2-nitronaphthalene (2NN), showing the NCI isosurfaces ($s = 0.5$) for values of sign(λ_2)ρ ranging from −0.025 to +0.025 a.u calculated at B3LYP-D3BJ/6–311++G(d,p) level of theory. The colours indicate interaction strength and type: blue for strong attractive interactions, green for weak attractive interactions, and red for repulsive interactions. The atom interaction distances are indicated (see text for discussion). **(b)** Results from QTAIM analyses for 1- and 2-nitronapthalene. Yellow spheres indicate bond critical points, orange spheres indicate ring critical points.

$$P^0(\text{Best}) = P^{eq}(\text{BDPCS3}) + \Delta P^{vib}(\text{HPCS2})$$
$$= P^{eq}(\text{BDPCS3}) + P^0(\text{HPCS2}) - P^{eq}(\text{HPCS2})$$

For both molecules, deuterium-substituted isotopologues are not available, preventing direct experimental information on hydrogen positions. Therefore, C–H bond lengths are fixed at their BDPCS3 values. Furthermore, the stability of the refinement process is strongly enhanced by grouping similar parameters in classes. In this approach (recently implemented in the MSR code) the differences between structural parameters belonging to the same class are held fixed at their initial (BDPCS3) values, so that a single parameter is optimized for each class. In the present case, all the C–C–C valence angles constitute a single class. Finally, the closeness of N–O bond lengths optimized at the BDPCS3 level with their SE counterparts for nitrobenzene (Table S1) makes it possible to freeze these parameters at their BDPCS3 values in the case of 1NN, where O isotopic substitutions are not available.

For 2NN (Table 4), the BDPCS3 equilibrium rotational constants augmented by HPCS2 vibrational corrections reproduce the experimental ground state rotational constants with a relative mean unsigned error approaching the so-called spectroscopic accuracy (average errors within 0.1%) and more than one order of magnitude smaller than its HPCS2 counterparts. Moreover, the agreement between computed and experimental NQCCs is remarkable, with vibrational corrections playing again a small, but non-negligible role. Several studies have shown that errors of this order of magnitude on spectroscopic parameters correspond to errors around 1 mÅ and 0.1° on equilibrium bond lengths and valence angles, respectively [53]. This accuracy, coupled with the availability of experimental results for all the isotopologues corresponding to single substitutions of non-hydrogen atoms and the grouping of all CCC valence angles in a single class, permits the determination of an accurate semi-experimental equilibrium structure retaining the hydrogen atom positions optimized at the BDPCS3 level. The results collected in Table 5 show that BDPCS3 and SE geometrical parameters are in remarkable agreement, giving further support to the proposed computational approach. Note that this level of accuracy is well above that of current studies for medium-sized molecules and comparable to that of state-of-the-art approaches for molecules containing 5–6 atoms.

1NN is a more complex case, since it has a non-planar equilibrium structure (hence a larger number of independent geometrical parameters) and there is no oxygen isotopic data available. The rotational constants computed at the HPCS2 level have larger errors than those obtained at the same level for 2NN (Table 6). However, "Best" results remain very accurate and can be confidently used to fix geometrical parameters not determinable from the experimental isotopic substitutions. The results reported in Table 7 show that a well-converged SE structure can be obtained also for 1NN and all the geometrical parameters are close to their BDPCS3 counterparts.

4. Discussion

The structural parameters corresponding to the various structures are collected in Tables 6 and 7. The r_s, $r_m^{(1)}$ and $r_e^{(SE)}$ structural parameters of 2NN show very good agreement, except for the r_s value of the C1–C9 bond length. This is probably due to the small values of the coordinates of atoms C1 and C9 (Table S3). In the case of 1NN, there are larger discrepancies between structures, with some r_s bond lengths considerably longer or shorter than the r_0 and $r_e^{(SE)}$ ones likely due to the small coordinates of several atoms, as indicated above.

As expected, in 1NN and 2NN the values of the C–C bond lengths are closer to those typical of a double bond (1.34 Å) than to a single bond (1.54 Å). Bonds C1–C2, C3–C4, C5–C6, and C7–C8 consistently show a stronger double bond character, with bond lengths around 1.37 Å. This behaviour follows that of naphthalene [72], and has also been observed in other substituted naphthalenes, such as 1-fluoronaphthalene [73], 1-chloronaphthalene [74], and 1- and 2-naphthol [75]. The bond angles for both nitronaphthalenes are all close to 120°. However, the angles involving the substituted position, ∠C9-C1-C2 in 1NN and ∠C1-C2-C3 in 2NN, increase by about 1–3° due to the substituent effect, while adjacent angles decrease by 2–3°. These changes induced by a ring substituent were evident in 1-fluoro- and 1-chloronaphthalene [73,74], with subtler effects reported for 1- and 2-naphthol [75].

The experimental value of the inertial defect $\Delta = -0.765(1)$ uÅ^2 for 2NN is the largest of all reported planar substituted naphthalenes. Non-zero values of the inertial defect arise from out-of-plane vibrational contributions, typically from the lower frequency modes. Several empirical expressions have been proposed to account for it by considering the lower-frequency modes and contributions from in-plane

vibrations proportional to the square root of I_c. The first expression suggested by Oka [65] was later refined by Gruet et al. [66] and Jahn et al. [67] for polycyclic molecules. The latter proposed to include not only the lowest out-of-plane vibrational mode but the same number of modes as the number of rings in the molecule, or + 1 for those molecules with an extra low out-of-plane vibration (normally below 100 cm^{-1}), using the expression:

$$\Delta_0 = \sum_{i=1}^{n} \frac{37.715\ \text{uÅ}^2}{\nu_i\ \text{cm}^{-1}} + 0.00107\sqrt{I_c}\ \text{uÅ}^2$$

Harmonic calculations performed at the B3LYP-D3BJ/6–311++G(d,p) level on the equilibrium structure yielded frequencies of 46.3 and 91.9 cm^{-1} for the two lowest out-of-plane vibrational modes. When these values are inserted into the empirical expression above, an inertial defect of $\Delta_0 = -0.718$ uÅ^2 is obtained. In the framework of VPT2, the inertial defect Δ_0 can be written as the sum of a Coriolis contribution, $-\Sigma_k[(\zeta^2_{a,k} + \zeta^2_{b,k} - \zeta^2_{c,k})/\omega_k]$, and an anharmonic contribution, $\Sigma_k\ \Sigma_i[F_{kki}/(\omega_k\omega_i)]$, where k runs over out-of-plane modes and i over totally symmetric modes. Within this framework, the inertial defect computed at the HPCS2 level amounts to $\Delta_0 = -0.716$ uÅ^2, in excellent agreement with experiment and without the introduction of any empirical correction. The inertial defect Δ_0 thus provides an independent validation of the HPCS2 vibrational force field, while the full set of rotational constants discussed above assesses the BDPCS3//HPCS2 model as a whole.

Finally, a noncovalent interaction (NCI) analysis [76,77] was performed on 1NN and 2NN (Fig. 3) to further our understanding of the factors influencing their structures and visualise possible intramolecular interactions by generating molecular electron gradient isosurfaces based on electron density and its derivatives. The NCI plots revealed attractive interactions in both molecules between the oxygen lone pairs of the nitro group and the neighbouring hydrogens depicted by bluish green isosurfaces. However, when performing QTAIM analysis [78], only 1NN showed a bond critical point between O1 and H8, indicating the presence of a C–H···O hydrogen bond (Fig. 3). The other weak attractive interactions occur at longer distances, which is likely to explain the differences between NCI and QTAIM analysis, as noted for other molecular systems [79].

5. Conclusions

The high-resolution rotational spectra of 1- and 2-nitronaphthalene have been recorded for the first time, providing access to precise experimental spectroscopic constants for heavy-atom isotopologues at natural abundance. From the analysis of isotopic data, the experimental r_s substitution structures have been obtained for both 1NN and 2NN. Moreover, an effective r_0 structure for 1NN and a mass-dependent $r_m^{(1)}$ structure for 2NN have also been determined. 2NN was found to be planar, while in 1NN the oxygens of the nitro group are off the molecular plane due to the steric interaction with the hydrogens of the naphthalene ring. Examination of the structural parameters of 1NN and 2NN with respect to those of related compounds revealed shared trends.

By integrating the experimental isotopic data with vibrational corrections computed from a cost-effective variant of the Pisa Composite Schemes (HPCS2), we have derived semi-experimental equilibrium geometries for 1NN and 2NN with spectroscopic accuracy. Despite the unavailability of deuterated isotopologues, the use of constrained hydrogen positions and analytically derived vibrational corrections allows reliable structural refinement from partial isotopic datasets. The results confirm the robustness of the semi-experimental approach and the reliability of PCS-based models for structurally complex polycyclic systems.

This work not only provides accurate reference geometries for two prototypical nitroaromatic molecules but also establishes a generalizable framework for high-precision structure determination of medium-sized rigid molecules, even with partial isotopic experimental data. The synergy demonstrated between rotational spectroscopy and composite quantum-chemical methods paves the way for future investigations of functionalized aromatics and environmentally relevant species. In this context, the detailed structural characterization of 1NN and 2NN, along with their intramolecular interactions, is an essential step towards understanding how these molecules engage with other atmospheric compounds, such as water, and gaining insight into the interplay between intra- and intermolecular forces.

Declaration of competing interest

The authors declare that they have no known competing financial interests or personal relationships that could have appeared to influence the work reported in this paper.

Acknowledgements

S·B. and M.E.S. would like to thank funding from UE FP7 (grant PCIG12-GA-2012-334525), King's College London, and EPSRC (EP/X039420/1), and acknowledge use of King's Computational Research, Engineering and Technology Environment (CREATE; retrieved November 19, 2025 from doi:10.18742/rnvf-m076). S.B. thanks King's College London for a PGR International Scholarship. M. M. and V. B. thank Gaussian Inc. for an R&D grant.

Appendix A. Supplementary data

Supplementary data to this article can be found online at https://doi.org/10.1016/j.saa.2026.127663.

Data availability

Data will be made available on request.

References

[1] A.T. Lawal, Polycyclic aromatic hydrocarbons. A review, Cogent Environ. Sci. 3 (2017) 1339841, https://doi.org/10.1080/23311843.2017.1339841.
[2] I. Abbas, G. Badran, A. Verdin, F. Ledoux, M. Roumié, D. Courcot, G. Garçon, Polycyclic aromatic hydrocarbon derivatives in airborne particulate matter: sources, analysis and toxicity, Environ. Chem. Lett. 16 (2018) 439–475, https://doi.org/10.1007/s10311-017-0697-0.
[3] B.A.M. Bandowe, H. Meusel, Nitrated polycyclic aromatic hydrocarbons (nitro-PAHs) in the environment – a review, Sci. Total Environ. 581–582 (2017) 237–257, https://doi.org/10.1016/j.scitotenv.2016.12.115.
[4] A. Feilberg, R.M. Kamens, M.R. Strommen, T. Nielsen, Modeling the formation, decay, and partitioning of semivolatile nitro-polycyclic aromatic hydrocarbons (nitronaphthalenes) in the atmosphere, Atmos. Environ. 33 (1999) 1231–1243, https://doi.org/10.1016/S1352-2310(98)00275-1.
[5] R. Atkinson, S.M. Aschmann, J. Arey, B. Zielinska, Gas-phase atmospheric chemistry of 1- and 2-nitronapthalene and 1,4-naphthoquinone, Atmos. Environ. 23 (1989) 2679–2690, https://doi.org/10.1016/0004-6981(89)90548-9.
[6] J. Sasaki, S.M. Aschmann, E.S.C. Kwok, R. Atkinson, J. Arey, Products of the gas-phase OH and NO3 radical-initiated reactions of naphthalene, Environ. Sci. Technol. 31 (1997) 3173–3179, https://doi.org/10.1021/es9701523.
[7] V. Librando, A. Alparone, Z. Minniti, Computational study on dipole moment, polarizability and second hyperpolarizability of nitronaphthalenes, J. Mol. Struct. THEOCHEM 856 (2008) 105–111, https://doi.org/10.1016/j.theochem.2008.01.022.
[8] V. Librando, A. Alparone, Prediction of mutagenic activity of nitronaphthalene isomers by infrared and Raman spectroscopy, J. Hazard. Mater. 154 (2008) 1158–1165, https://doi.org/10.1016/j.jhazmat.2007.11.020.
[9] A. Giussani, G.A. Worth, Similar chemical structures, dissimilar triplet quantum yields: a CASPT2 model rationalizing the trend of triplet quantum yields in nitroaromatic systems, Phys. Chem. Chem. Phys. 21 (2019) 10514–10522, https://doi.org/10.1039/c9cp00705a.
[10] K.K. Onchoke, C.M. Hadad, P.K. Dutta, Density functional theoretical study of nitrated polycyclic aromatic hydrocarbons, Polycycl. Aromat. Compd. 24 (2004) 37–64, https://doi.org/10.1080/10406630490277443.
[11] J.P. Zobel, J.J. Nogueira, L. González, Mechanism of ultrafast intersystem crossing in 2-nitronaphthalene, Chem. – A Eur. J. 24 (2018) 5379–5387, https://doi.org/10.1002/chem.201705854.
[12] R.A. Vogt, C. Reichardt, C.E. Crespo-Hernández, Excited-state dynamics in nitronaphthalene derivatives: intersystem crossing to the triplet manifold in hundreds of

femtoseconds, J. Phys. Chem. A 117 (2013) 6580–6588, https://doi.org/10.1021/jp405656n.
[13] R.A. Vogt, C.E. Crespo-Hernández, Conformational control in the population of the triplet state and photoreactivity of nitronaphthalene derivatives, J. Phys. Chem. A 117 (2013) 14100–14108, https://doi.org/10.1021/jp4101587.
[14] P.T. Phousongphouang, J. Arey, Rate constants for the photolysis of the nitronaphthalenes and methylnitronaphthalenes, J. Photochem. Photobiol. A Chem. 157 (2003) 301–309, https://doi.org/10.1016/S1010-6030(03)00072-8.
[15] A. Feilberg, R.M. Kamens, M.R. Strommen, T. Nielsen, Photochemistry and partitioning of Semivolatile nitro-PAH in the atmosphere, Polycycl. Aromat. Compd. 14 (1999) 151–160, https://doi.org/10.1080/10406639908019121.
[16] R.M. Healy, Y. Chen, I. Kourtchev, M. Kalberer, D. Oshea, J.C. Wenger, Rapid formation of secondary organic aerosol from the photolysis of 1-nitronaphthalene: role of naphthoxy radical self-reaction, Environ. Sci. Technol. 46 (2012) 11813–11820, https://doi.org/10.1021/es302841j.
[17] E.K. Kim, T.M. Bockman, J.K. Kochi, The mechanism of charge-transfer nitration of naphthalene, J. Chem. Soc., Perkin Trans. 2 (1992) 1879–1891, https://doi.org/10.1039/P29920001879.
[18] S. Sankararaman, J.K. Kochi, Charge-transfer nitration of naphthalene and the methylnaphthalenes. Part 1. Direct comparison with electrophilic aromatic nitrations, J. Chem. Soc. Perkin Trans. 2 (1991) 1–12, https://doi.org/10.1039/P29910000001.
[19] W. Gordy, R.L. Cook, Microwave Molecular Spectra, Wiley, New York, 1984.
[20] S. Zinn, M. Schnell, Flexibility at the fringes: conformations of the steroid hormone β-Estradiol, ChemPhysChem 19 (2018) 2915–2920, https://doi.org/10.1002/cphc.201800647.
[21] S. Saxena, S. Panchagnula, M.E. Sanz, C. Pérez, L. Evangelisti, B.H. Pate, Structural changes induced by quinones: high-resolution microwave study of 1,4-naphthoquinone, ChemPhysChem 21 (2020) 2579–2584, https://doi.org/10.1002/cphc.202000665.
[22] A. Insausti, E.R. Alonso, S. Municio, I. León, L. Kolesniková, S. Mata, Determining the Molecular shape of progesterone: insights from laser ablation rotational spectroscopy, J. Phys. Chem. Lett. 16 (2025) 2425–2432, https://doi.org/10.1021/acs.jpclett.4c03618.
[23] Y. Li, F. Shen, Y. Feng, W. Lv, H. Huang, J. Huang, G. Feng, Rotational spectroscopy of 1,2-dihydronaphthalene, 1,4-dihydronaphthalene, and 1,2,3,4-tetrahydronaphthalene, J. Chem. Phys. 162 (2025) 134301, https://doi.org/10.1063/5.0257949.
[24] S. Di Grande, V. Barone, Toward accurate quantum chemical Methods for molecules of increasing dimension: the new family of Pisa composite schemes, J. Phys. Chem. A 128 (2024) 4886–4900, https://doi.org/10.1021/acs.jpca.4c01673.
[25] V. Barone, From perception to prediction and interpretation: enlightening the Gray zone of Molecular bricks of life with the help of machine learning and quantum chemistry, WIREs Comput. Mol. Sci. 15 (2025) e70000, https://doi.org/10.1002/wcms.70000.
[26] M. Mendolicchio, V. Barone, Unbiased comparison between theoretical and experimental Molecular structures and properties: toward an accurate reduced-cost evaluation of vibrational contributions, J. Chem. Theory Comput. 20 (2024) 2842–2857, https://doi.org/10.1021/acs.jctc.4c00023.
[27] M. Mendolicchio, V. Barone, Accurate vibrational and Ro-vibrational contributions to the properties of large molecules by a new engine employing curvilinear internal coordinates and vibrational perturbation theory to second order, J. Chem. Theory Comput. 20 (2024) 8378–8395, https://doi.org/10.1021/acs.jctc.4c00857.
[28] M.J. Frisch, G.W. Trucks, H.B. Schlegel, G.E. Scuseria, M.A. Robb, J.R. Cheeseman, G. Scalmani, V. Barone, G.A. Petersson, H. Nakatsuji, X. Li, M. Caricato, A. V. Marenich, J. Bloino, B.G. Janesko, R. Gomperts, B. Mennucci, H.P. Hratchian, J. V. Ortiz, A.F. Izmaylov, J.L. Sonnenberg, D. Williams-Young, F. Ding, F. Lipparini, F. Egidi, J. Goings, B. Peng, A. Petrone, T. Henderson, D. Ranasinghe, V. G. Zakrzewski, J. Gao, N. Rega, G. Zheng, W. Liang, M. Hada, M. Ehara, K. Toyota, R. Fukuda, J. Hasegawa, M. Ishida, T. Nakajima, Y. Honda, O. Kitao, H. Nakai, T. Vreven, K. Throssell, J.J.A. Montgomery, J.E. Peralta, F. Ogliaro, M.J. Bearpark, J.J. Heyd, E.N. Brothers, K.N. Kudin, V.N. Staroverov, T.A. Keith, R. Kobayashi, J. Normand, K. Raghavachari, A.P. Rendell, J.C. Burant, S.S. Iyengar, J. Tomasi, M. Cossi, J.M. Millam, M. Klene, C. Adamo, R. Cammi, J.W. Ochterski, R.L. Martin, K. Morokuma, O. Farkas, J.B. Foresman, D.J. Fox, Gaussian16, Revision B.01, Gaussian, Inc., Wallingford CT., 2016.
[29] M. Mendolicchio, E. Penocchio, D. Licari, N. Tasinato, V. Barone, Development and implementation of advanced fitting Methods for the calculation of accurate Molecular structures, J. Chem. Theory Comput. 13 (2017) 3060–3075, https://doi.org/10.1021/acs.jctc.7b00279.
[30] P. Pulay, W. Meyer, J.E. Boggs, Cubic force constants and equilibrium geometry of methane from Hartree–Fock and correlated wavefunctions, J. Chem. Phys. 68 (1978) 5077–5085, https://doi.org/10.1063/1.435626.
[31] J. Demaison, Experimental, semi-experimental andab initio equilibrium structures, Mol. Phys. 105 (2007) 3109–3138, https://doi.org/10.1080/00268970701765811.
[32] M. Piccardo, E. Penocchio, C. Puzzarini, M. Biczysko, V. Barone, Semi-experimental equilibrium structure determinations by employing B3LYP/SNSD anharmonic force fields: validation and application to semirigid organic molecules, J. Phys. Chem. A 119 (2015) 2058–2082, https://doi.org/10.1021/jp511432m.
[33] E. Penocchio, M. Piccardo, V. Barone, Semiexperimental equilibrium structures for building blocks of organic and biological molecules: the B2PLYP route, J. Chem. Theory Comput. 11 (2015) 4689–4707, https://doi.org/10.1021/acs.jctc.5b00622.
[34] G.G. Brown, B.C. Dian, K.O. Douglass, S.M. Geyer, S.T. Shipman, B.H. Pate, A broadband Fourier transform microwave spectrometer based on chirped pulse excitation, Rev. Sci. Instrum. 79 (2008) 1–13, https://doi.org/10.1063/1.2919120.
[35] V. Barone, Accuracy meets feasibility for the structures and rotational constants of the Molecular bricks of life: a joint venture of DFT and wave-function Methods, J. Phys. Chem. Lett. 14 (2023) 5883–5890, https://doi.org/10.1021/acs.jpclett.3c01380.
[36] V. Barone, PCS/bonds and PCS0: pick your molecule and get its accurate structure and ground state rotational constants at DFT cost, J. Chem. Phys. 159 (2023) 81102, https://doi.org/10.1063/5.0167296.
[37] D. Loru, M.A. Bermúdez, M.E. Sanz, Structure of fenchone by broadband rotational spectroscopy, J. Chem. Phys. 145 (2016) 074311, https://doi.org/10.1063/1.4961018.
[38] D. Loru, M.M. Quesada-Moreno, J.R. Avilés-Moreno, N. Jarman, T.R. Huet, J. J. López-González, M.E. Sanz, Conformational flexibility of limonene oxide studied by microwave spectroscopy, ChemPhysChem 18 (2017) 268, https://doi.org/10.1002/cphc.201700042.
[39] C. Lee, W. Yang, R.G. Parr, Development of the Colle-Salvetti correlation-energy formula into a functional of the electron density, Phys. Rev. B 37 (1988) 785–789, https://doi.org/10.1103/PhysRevB.37.785.
[40] A.D. Becke, Thermochemistry. III. The role of exact exchange, J. Chem. Phys. 98 (1993) 5648–5652, https://doi.org/10.1063/1.464913.
[41] S. Grimme, J. Antony, S. Ehrlich, H. Krieg, A consistent and accurate ab initio parametrization of density functional dispersion correction (DFT-D) for the 94 elements H-Pu, J. Chem. Phys. 132 (2010) 154104, https://doi.org/10.1063/1.3382344.
[42] S. Grimme, S. Ehrlich, L. Goerigk, Effect of the damping function in dispersion corrected density functional theory, J. Comput. Chem. 32 (2011) 1456–1465, https://doi.org/10.1002/jcc.21759.
[43] C. Møller, M.S. Plesset, Note on an approximation treatment for many-electron systems, Phys. Rev. 46 (1934) 618–622, https://doi.org/10.1103/PhysRev.46.618.
[44] J.B. Graneek, W.C. Bailey, M. Schnell, Electron-withdrawing effects on the molecular structure of 2- and 3-nitrobenzonitrile revealed by broadband rotational spectroscopy and their comparison with 4-nitrobenzonitrile, Phys. Chem. Chem. Phys. 20 (2018) 22210–22217, https://doi.org/10.1039/c8cp01539b.
[45] A. Roucou, I. Kleiner, M. Goubet, S. Bteich, G. Mouret, R. Bocquet, F. Hindle, W. L. Meerts, A. Cuisset, Towards the detection of explosive taggants: microwave and millimetre-wave gas-phase spectroscopies of 3-nitrotoluene, ChemPhysChem 19 (2018) 1056–1067, https://doi.org/10.1002/cphc.201701266.
[46] A. Roucou, M. Goubet, I. Kleiner, S. Bteich, A. Cuisset, Large amplitude torsions in nitrotoluene isomers studied by rotational spectroscopy and quantum chemistry calculations, ChemPhysChem 21 (2020) 2523–2538, https://doi.org/10.1002/cphc.202000591.
[47] S. Baweja, E. Antonelli, S. Hussain, A. Fernández-Ramos, I. Kleiner, H.V.L. Nguyen, M.E. Sanz, Revealing internal rotation and 14N nuclear quadrupole coupling in the atmospheric pollutant 4-Methyl-2-nitrophenol: interplay of microwave spectroscopy and quantum chemical calculations, Molecules 28 (2023), https://doi.org/10.3390/molecules28052153.
[48] E. Sicilia, G. De Luca, S. Chiodo, N. Russo, P. Calaminici, A.M. Koster, K. Jug, Density functional theory calculations of nuclear quadrupole coupling constants with calibrated 14N quadrupole moments, Mol. Phys. 99 (2001) 1039–1051, https://doi.org/10.1080/00268970110042820.
[49] W.J. Hehre, R. Ditchfield, J.A. Pople, Self—consistent molecular orbital methods. XII. Further extensions of gaussian—type basis sets for use in molecular orbital studies of organic molecules, J. Chem. Phys. 56 (1972) 2257–2261, https://doi.org/10.1063/1.1677527.
[50] P.C. Hariharan, J.A. Pople, The influence of polarization functions on molecular orbital hydrogenation energies, Theor. Chim. Acta 28 (1973) 213–222, https://doi.org/10.1007/BF00533485.
[51] T. Clark, J. Chandrasekhar, G.W. Spitznagel, P.V.R. Schleyer, Efficient diffuse function-augmented basis sets for anion calculations. III. The 3-21+G basis set for first-row elements, Li–F, J. Comput. Chem. 4 (1983) 294–301, https://doi.org/10.1002/jcc.540040303.
[52] G. Santra, N. Sylvetsky, J.M.L. Martin, Minimally empirical double-hybrid functionals trained against the GMTKN55 database: revDSD-PBEP86-D4, revDOD-PBE-D4, and DOD-SCAN-D4, J. Phys. Chem. A 123 (2019) 5129–5143, https://doi.org/10.1021/acs.jpca.9b03157.
[53] V. Barone, Quantum chemistry meets high-resolution spectroscopy for characterizing the molecular bricks of life in the gas-phase, Phys. Chem. Chem. Phys. 26 (2024) 5802–5821, https://doi.org/10.1039/D3CP05169B.
[54] K.A. Peterson, T.B. Adler, H.-J. Werner, Systematically convergent basis sets for explicitly correlated wavefunctions: the atoms H, He, B–Ne, and Al–Ar, J. Chem. Phys. 128 (2008) 84102, https://doi.org/10.1063/1.2831537.
[55] T.H. DunningJr, Gaussian basis sets for use in correlated molecular calculations. I. The atoms boron through neon and hydrogen, J. Chem. Phys. 90 (1989) 1007–1023, https://doi.org/10.1063/1.456153.
[56] G. Ceselin, V. Barone, N. Tasinato, Accurate biomolecular structures by the Nano-LEGO approach: pick the bricks and build your geometry, J. Chem. Theory Comput. 17 (2021) 7290–7311, https://doi.org/10.1021/acs.jctc.1c00788.
[57] V. Barone, G. Ceselin, M. Fusè, N. Tasinato, Accuracy meets interpretability for computational spectroscopy by means of Hybridand double-hybrid functionals, Front. Chem. 8 (2020) 584203, https://doi.org/10.3389/fchem.2020.584203.
[58] D. Hait, M. Head-Gordon, How accurate is density functional theory at predicting dipole moments? An assessment using a new database of 200 benchmark values, J. Chem. Theory Comput. 14 (2018) 1969–1981, https://doi.org/10.1021/acs.jctc.7b01252.

[59] V. Barone, M. Fusè, F. Lazzari, G. Mancini, Benchmark structures and conformational landscapes of amino acids in the gas phase: a joint venture of machine learning, quantum chemistry, and rotational spectroscopy, J. Chem. Theory Comput. 19 (2023) 1243–1260, https://doi.org/10.1021/acs.jctc.2c01143.
[60] N.A. Seifert, I.A. Finneran, C. Perez, D.P. Zaleski, J.L. Neill, A.L. Steber, R. D. Suenram, A. Lesarri, S.T. Shipman, B.H. Pate, AUTOFIT, an automated fitting tool for broadband rotational spectra, and applications to 1-hexanal, J. Mol. Spectrosc. 312 (2015) 13–21, https://doi.org/10.1016/j.jms.2015.02.003.
[61] C.M. Western, B.E. Billinghurst, Automatic and semi-automatic assignment and fitting of spectra with PGOPHER, Phys. Chem. Chem. Phys. 21 (2019) 13986–13999, https://doi.org/10.1039/c8cp06493h.
[62] C.M. Western, PGOPHER: a program for simulating rotational, vibrational and electronic spectra, J. Quant. Spectrosc. Radiat. Transf. 186 (2017) 221–242, https://doi.org/10.1016/j.jqsrt.2016.04.010.
[63] H.M. Pickett, The fitting and prediction of vibration-rotation spectra with spin interactions, J. Mol. Spectrosc. 148 (1991) 371–377, https://doi.org/10.1016/0022-2852(91)90393-O.
[64] J.K.G. Watson, Vibrational Spectra and Structure 6, Elsevier, New York, 1977, https://doi.org/10.1016/0022-2860(78)87040-9.
[65] T. Oka, On negative inertial defect, J. Mol. Struct. 352–353 (1995) 225–233, https://doi.org/10.1016/0022-2860(95)08844-L.
[66] S. Gruet, M. Goubet, O. Pirali, High resolution measurements supported by electronic structure calculations of two naphthalene derivatives: [1,5]- and [1,6]-naphthyridine - estimation of the zero point inertial defect for planar polycyclic aromatic compounds, J. Chem. Phys. 140 (2014) 234308, https://doi.org/10.1063/1.4882652.
[67] M.K. Jahn, J.U. Grabow, M.J. Travers, D. Wachsmuth, P.D. Godfrey, D. McNaughton, The radio spectra of planar aromatic heterocycles: how to quantify and predict the negative inertial defects, Phys. Chem. Chem. Phys. 19 (2017) 8970–8976, https://doi.org/10.1039/c6cp07487a.
[68] J. Kraitchman, Determination of Molecular structure from microwave spectroscopic data, Am. J. Phys. 21 (1953) 17–24, https://doi.org/10.1119/1.1933338.
[69] Z. Kisiel, Assignment and analysis of complex rotational spectra, Spectrosc. from Sp. (2001) 91–106, https://doi.org/10.1007/978-94-010-0832-7_6.
[70] J.K.G. Watson, A. Roytburg, W. Ulrich, Least-squares mass-dependence Molecular structures, J. Mol. Spectrosc. 196 (1999) 102–119, https://doi.org/10.1006/jmsp.1999.7843.
[71] O.V. Dorofeeva, Y.V. Vishnevskiy, N. Vogt, J. Vogt, L.V. Khristenko, S. V. Krasnoshchekov, I.F. Shishkov, I. Hargittai, L.V. Vilkov, Molecular structure and conformation of nitrobenzene reinvestigated by combined analysis of gas-phase electron diffraction, rotational constants, and theoretical calculations, Struct. Chem. 18 (2007) 739–753, https://doi.org/10.1007/s11224-007-9186-6.
[72] H. Sellers, J.E. Boggs, The structure of naphthalene, J. Mol. Struct. 74 (1981) 137–142, https://doi.org/10.1016/0022-2860(81)80014-2.
[73] S. Gupta, C.N. Cummings, N.R. Walker, E. Arunan, Revisiting the microwave spectrum and molecular structure of 1-fluoronaphthalene, J. Mol. Spectrosc. 407 (2025) 111968, https://doi.org/10.1016/j.jms.2024.111968.
[74] P. Pinacho, P. Gómez, J.C. López, S. Blanco, Accurate experimental structure of 1-Chloronaphthalene, ChemPhysChem 25 (2024) e202400072, https://doi.org/10.1002/cphc.202400072.
[75] A.S. Hazrah, S. Nanayakkara, N.A. Seifert, E. Kraka, W. Jäger, Structural study of 1- and 2-naphthol: new insights into the non-covalent H–H interaction in cis-1-naphthol, Phys. Chem. Chem. Phys. 24 (2022) 3722–3732, https://doi.org/10.1039/D1CP05632H.
[76] J. Contreras-García, E.R. Johnson, S. Keinan, R. Chaudret, J.P. Piquemal, D. N. Beratan, W. Yang, NCIPLOT: a program for plotting noncovalent interaction regions, J. Chem. Theory Comput. 7 (2011) 625–632, https://doi.org/10.1021/ct100641a.
[77] R. Chaudret, B. De Courcy, J. Contreras-García, E. Gloaguen, A. Zehnacker-Rentien, M. Mons, J.P. Piquemal, Unraveling non-covalent interactions within flexible biomolecules: from electron density topology to gas phase spectroscopy, Phys. Chem. Chem. Phys. 16 (2014) 9876–9891, https://doi.org/10.1039/c3cp52774c.
[78] R.F.W. Bader, A quantum theory of Molecular structure and its applications, Chem. Rev. 91 (1991) 893–928, https://doi.org/10.1021/cr00005a013.
[79] S. Indira Murugachandran, I. Peña, A. Mokhtar Lamsabhi, M. Yáñez, M. Eugenia Sanz, Alcohol Self-aggregation: the preferred configurations of the ethanol trimer, Angew. Chemie Int. Ed. 64 (2025) e202415229, https://doi.org/10.1002/anie.202415229.